

Kinetics of the Formation of a Phospholipid Multilayer on a Silica Sol Surface

A. M. Tikhonov^{a,*}, V. E. Asadchikov^b, Yu. O. Volkov^b, B. S. Roshchin^b,
I. S. Monakhov^c, and I. S. Smirnov^c

^a Kapitza Institute for Physical Problems, Russian Academy of Sciences, Moscow, 119334 Russia

^b Federal Research Center Crystallography and Photonics, Russian Academy of Sciences, Moscow, 119333 Russia

^c National Research University Higher School of Economics, Moscow, 101000 Russia

*e-mail: tikhonov@kapitza.ras.ru

Received October 12, 2016

The ordering of a multilayer consisting of DSPC bilayers on a silica sol substrate is studied within the model-independent approach to the reconstruction of profiles of the electron density from X-ray reflectometry data. It is found that the electroporation of bilayers in the field of anion silica nanoparticles significantly accelerates the process of their saturation with Na^+ and H_2O , which explains both a relatively small time of formation of the structure of the multilayer of $1\text{--}7 \times 10^5$ s and $\sim 13\%$ excess of the electron density in it.

DOI: 10.1134/S0021364016240139

A bilayer of phospholipid molecules is considered as the simplest model of a cell membrane [1–5]. We previously observed the crystallization of a multilayer of phospholipid bilayers whose thickness is given by the Debye screening length Λ_D in the bulk of a hydrosol substrate on the surface of the aqueous solution of amorphous silicon dioxide nanoparticles [6, 7] (Fig. 1). In this work, the ordering of the multilayer is studied within the model-independent approach to the reconstruction of profiles of the electron density from X-ray reflectometry data without any a priori assumptions on the structure of the multilayer [8–12]. According to our data, the characteristic time of formation of the structure of the surface is $10^5\text{--}7 \times 10^5$ s; after that, the lipid film can be considered as a two-dimensional organic crystal with a quite high degree of perfection.

We study multilayers of 1,2-distearoyl-sn-glycero-3-phosphocholine (DSPC) or $\text{C}_{44}\text{H}_{88}\text{NO}_8\text{P}$ [2]. The hydrophobic part of the DSPC molecule consists of two hydrocarbon chains of 18 carbon atoms and has a length of ≈ 2 nm, whereas the hydrophilic part consists of glycerol and phosphocholine and has a length of ≈ 1.5 nm.

Concentrated monodisperse hydrosols of SiO_2 nanoparticles stabilized by sodium hydroxide—Ludox SM-30 (with the diameter of nanoparticles ~ 7 nm and the weight fractions of SiO_2 and NaOH of 30 and 0.5 wt %, respectively, and $\text{pH} \approx 10$) and Ludox HS-

40 (with the diameter of nanoparticles ~ 12 nm and the weight fractions of SiO_2 and NaOH of 40 and 0.4 wt %, respectively, and $\text{pH} \approx 9.5$)—were used as substrates [13–16]. The DSPC synthetic phospholipid and silica hydrosols were purchased from Avanti Polar Lipids Inc. and Grace Davison Co., respectively.

The used silica solutions had the parameter $\Lambda_D = \sqrt{\epsilon_0 \epsilon k_B T / (N_A e^2 c^-)} \approx 400$ Å, where $\epsilon_0 \approx 8.85 \times 10^{-12}$ F/m is the permittivity of free space, $\epsilon \approx 80$ is

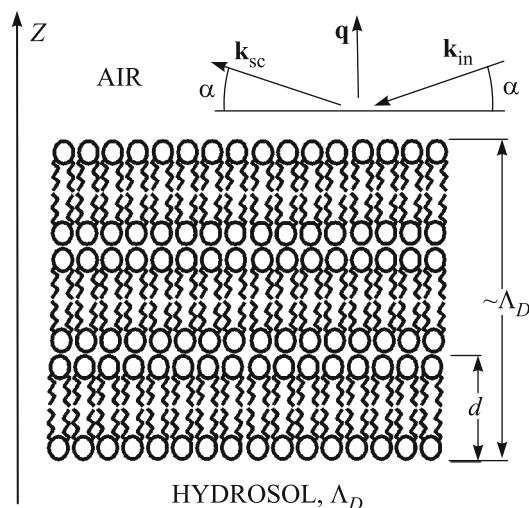


Fig. 1. Multilayer of phospholipid bilayers.

the dielectric constant of water, $k_B \approx 1.38 \times 10^{-23}$ J/K is the Boltzmann constant, $T \approx 298$ K is the temperature, $N_A \approx 6.02 \times 10^{23}$ mol⁻¹ is the Avogadro number, $e \approx 1.6 \times 10^{-19}$ C is the elementary charge, and $c^- \approx 10^{-4}$ mol/L is the concentration of free OH⁻ ions in the sol at pH = 10 [17, 18]. Because of a small difference in pH, the parameter Λ_D for the solution of 12-nm silica particles is larger than that for the solution of 7-nm particles by ~40%.

According to the size distribution of nanoparticles found from the intensity of small-angle scattering, the characteristic diameter of particles in the solution is ~30% larger than the value declared by the manufacturer [19, 20].

The multilayer samples were prepared and studied in a air tight cell with X-ray-transparent windows according to the method described in [6]. One or two drops of the solution of phospholipid in chloroform ($\sim 5 \times 10^{-2}$ mol/L) with a total volume of ~10 μ L were deposited by a syringe on the surface of the liquid freshly prepared hydrosol substrate placed in a polytetrafluoroethylene dish with a diameter of 100 mm. In this manner, a multilayer of 10–20 lipid monolayers can be formed on the surface. At such deposition of the surfactant, its excess is accumulated in three-dimensional aggregates in equilibrium with the phospholipid film.

The transverse structure of the lipid layer was studied by the X-ray reflectometry method on a multipurpose laboratory diffractometer with a mobile emitter–detector system [21]. An X-ray tube with a copper anode was used as the emitter. The $K\alpha_1$ line (photon energy $E = 8048$ eV and wavelength $\lambda = (1.5405 \pm 0.0001)$ Å) was separated from the tube radiation spectrum by means of a single Si (111) crystal monochromator. The vertical and horizontal dimensions of the beam were ~0.1 and ~8 mm, respectively. The three-slit collimation system forms a probe X-ray beam with the angular width in the plane of incidence $\sim 10^{-4}$ rad. The angular resolution of the point detector was $\sim 1.7 \times 10^{-3}$ rad and is determined by the input slit with a gap of 1 mm at a distance of ~570 mm from the center of the sample. To reduce the absorption and scattering of radiation in air, we used vacuum paths with X-ray-transparent windows.

At specular reflection, the scattering vector $\mathbf{q} = \mathbf{k}_{in} - \mathbf{k}_{sc}$, where \mathbf{k}_{in} and \mathbf{k}_{sc} are the wave vectors of the incident and scattered rays in the direction to the observation point, respectively, has only one nonzero component $q_z = (4\pi/\lambda)\sin\alpha$, where α is the glancing angle in the plane normal to the surface (see Fig. 1). The software of the diffractometer allows specifying a variable angular step, width of the slit of the detector,

and time of exposure, which makes it possible to optimize the measurement of the reflection coefficient R , which decreases rapidly with an increase in α .

Experimental data were processed with a correction to the shape of the probe X-ray beam because only a part of the beam reaches the sample surface in the region of small angles. The background begins to significantly affect the angular dependence of the reflection coefficient at large angles. This effect was taken into account by the subtraction of the previously measured average value in this angular range, which was ~0.1 pulses/s. Thus, the data for the reflection coefficient $R(q_z)$ obtained on the diffractometer are comparable in spatial resolution $2\pi/q_z^{\max} \approx 10$ Å (where $q_z^{\max} \approx 0.5$ Å⁻¹ is the maximum q_z value in the experiment) with the data previously obtained with synchrotron radiation [6, 7].

Figure 2 shows the experimental dependences of the reflectivity $R(q_z)$ from the surface of clean boundaries of silica sols of (circles, squares) 7-nm and (diamonds, triangles) 12-nm particles. All curves exhibit a characteristic feature near $q_z \approx 0.05$ Å⁻¹, which is due to the separation of the components of the substrate at the (air–silica sol) interface [22].

Figure 3 shows data for the reflection coefficient $R(q_z)$ from the DSPC phospholipid film depos-

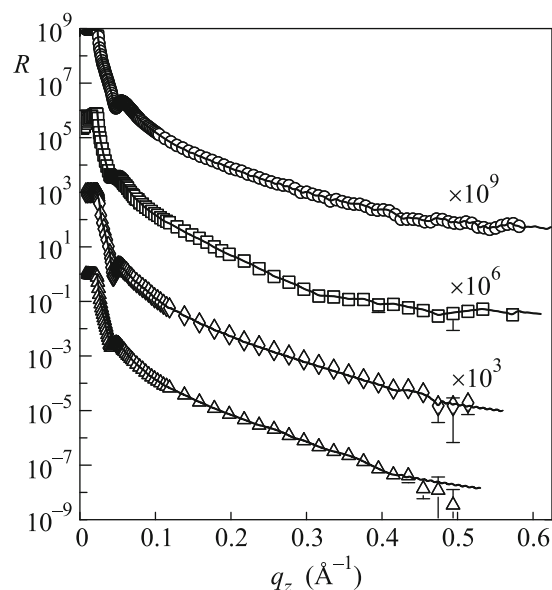


Fig. 2. Dependence $R(q_z)$ for the silica sol surface: circles correspond to the solution of 7-nm particles immediately after the preparation of the sample, squares are data for this solution after ~170 h, diamonds correspond to the solution of 12-nm particles immediately after the preparation of the sample, and triangles are data for this solution after ~130 h. The lines are fits for the reconstruction of the electron density profiles.

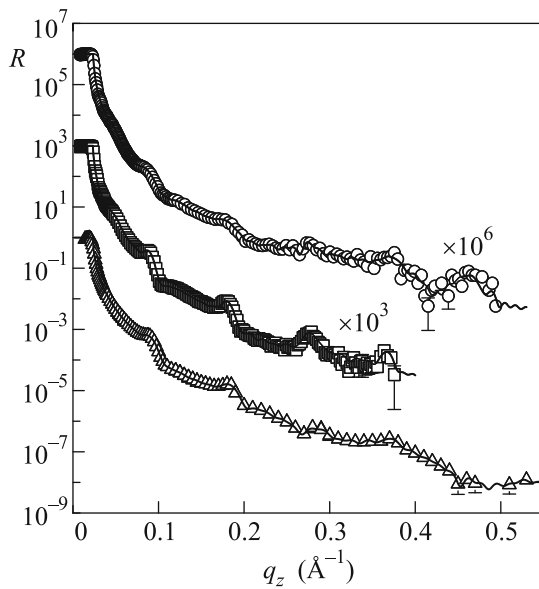


Fig. 3. Reflectivity curves $R(q_z)$ from the DSPC film on the surface of the solution of 7-nm particles measured (circles) immediately after deposition, (squares) after ~ 24 h, and (triangles) after ~ 100 h. The lines are fits for the reconstruction of the electron density profiles.

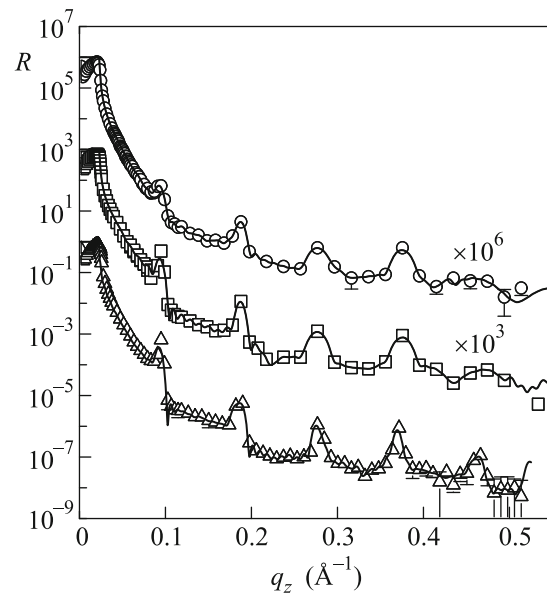


Fig. 4. Reflectivity curves $R(q_z)$ from the DSPC film on the surface of silica sol of 12-nm particles measured after (circles) 24, (squares) ~ 70 , and (triangles) ~ 200 h. The lines are fits for the reconstruction of the electron density profiles.

ited on the substrate of the silica sol of 7-nm particles. Circles correspond to reflection from the sample during the first hour. The characteristic feature near $q_z \approx 0.05 \text{ \AA}^{-1}$ has an inverted shape: a weakly pronounced maximum is observed instead of the minimum intensity, which indicates a significant rearrangement of the separation region. The squares show the reflection coefficient from the same sample ~ 24 h after the deposition of the lipid. This curve exhibits a regular set of reflection peaks with the oscillation period $\Delta q_z = (0.094 \pm 0.007) \text{ \AA}^{-1}$, which corresponds to an ordered structure with an estimated period of $2\pi/\Delta q_z = (66.8 \pm 4.5) \text{ \AA}$. The triangles show the reflection coefficient from the DSPC lipid multilayer aged for ~ 100 h. The shape of the reflection peaks and their period $\Delta q_z = (0.096 \pm 0.012) \text{ \AA}^{-1}$ almost coincide with the shape and period of the peaks on the preceding curve.

Figure 4 shows the dependences $R(q_z)$ for the thick DSPC phospholipid multilayer which was formed on the substrate of the silica sol of 12-nm particles. The measurements were performed at (circles) ~ 24 h, (squares) ~ 70 h, and (triangles) ~ 200 h after the preparation of the sample. As in the preceding case, regular reflection peaks narrowing with the time with a step of $\Delta q_z = (0.096 \pm 0.009) \text{ \AA}^{-1}$ are seen on all curves.

At the measurement of $R(q_z)$, the contribution of lateral inhomogeneities of the structure is statistically

averaged over the illumination spot on the sample whose characteristic area was $S \approx 100 \text{ mm}^2$. For this reason, the structure of the surface layer of the samples can be considered in the approximation of an ideal inhomogeneous-layered structure. To analyze the reflectometry data, we used the model-independent approach proposed by Kozhevnikov [8, 11]. A significant advantage of this approach is that it does not require any a priori assumptions on the shape of the structure under study, in contrast to the widely used model approach [23–27].

The model-independent approach is based on the extrapolation of the asymptotic behavior of the reflectivity curve $R(q_z)$ to the region of high q_z values under the assumption that the distribution of the polarizability across the surface of the sample $\delta(z)$ or its derivatives have jumps at the points z_j [11, 12]. If all distances between z_j are different, only two physically reasonable distributions $\delta(z)$ correspond to the reflection coefficient $R(q_z)$ measured in a limited range of q_z . These distributions differ from each other in the arrangement of the points z_j with respect to the boundary of the substrate. Further, we chose the solution at which the first point of discontinuity $z_1 = 0$ corresponds to the air–multilayer interface and the other points z_j are deep in the substance ($z_j < 0$). To describe the studied samples, it appeared to be sufficient to consider only the points of discontinuity of the zeroth and first orders, i.e., jumps in the function $\delta(z)$

and its derivative $\delta'(z)$, respectively. The profiles $\delta(z)$ were numerically optimized by fitting the calculated reflection curve (the function $\delta(z)$ and q_z) to the experimental data for $R(q_z)$ with the use of the standard Levenberg–Marquardt algorithm [28].

For weakly absorbing substances, in the spectral range of hard X rays, the model-independent depth profiles of the electron density $\rho(z) \approx \pi\delta(z)/(r_0\lambda^2)$, where $r_0 = 2.814 \times 10^{-5} \text{ \AA}$ is the classical radius of the electron [29], can be calculated from the reconstructed distributions of the optical constant $\delta(z)$. Then, by comparing the reconstructed profile $\rho(z)$ with a certain structural model of the surface layer, the specific area A per structural unit (ion, molecule, or chemical group) in the layer with the thickness $d = z_2 - z_1$ can be estimated as

$$A = \frac{\Gamma}{z_2 - z_1} \frac{\int_{z_1}^{z_2} \rho(z) dz}{\rho_w}, \quad (1)$$

where Γ is the number of electrons in the structural unit. For example, for the DSPC molecule, $\Gamma = 438$.

All dependences $R(q_z)$ in Fig. 2 decrease as $\propto 1/q_z^4$. Further analysis shows that the function $\delta(z)$ has only one singular point of the zeroth order. Figure 5a shows the reconstructed profiles $\rho(z)$ in the surface of the layer of the sol of 7-nm particles divided by the electron density in water under normal conditions $\rho_w = 0.333 \text{ electrons/\AA}^3$. They qualitatively correspond to the model of electric double layer proposed in [17, 18]. The thickness of the densest layer (loose nanoparticle monolayer) with a maximum at a depth of $\sim 150 \text{ \AA}$ was $\approx 100 \text{ \AA}$ and approximately corresponds to the diameter of SiO_2 nanoparticles in the sol. Immediately after the preparation of the sample (dashed line), the maximum electron density in this layer is $\rho_{\text{max}} \approx 1.3\rho_w$, which is $\sim 12\%$ larger than the value in the bulk of the solution $\rho_b \approx 1.15\rho_w$; i.e., the concentration of nanoparticles in this layer is larger than the bulk value by a factor of $(\rho_{\text{max}} - \rho_w)/(\rho_b - \rho_w) \approx 2$. The second layer with the same thickness and the concentration of silicon dioxide particles exceeding the bulk value by $\sim 20\%$ is simultaneously observed at a larger depth. The total thickness of the observed separation region reaches $\sim 500 \text{ \AA}$.

After the aging of the sample for $\sim 170 \text{ h}$ (solid line in Fig. 5a), the concentration of nanoparticles in the loose multilayer decreases by $\sim 20\%$, its position is shifted deeper in the substrate, and the second layer disappears. The total thickness of the separation layer decreases to $\sim 300 \text{ \AA}$, which is in agreement with the estimate $\Lambda_D \approx 400 \text{ \AA}$ for this solution. A narrow

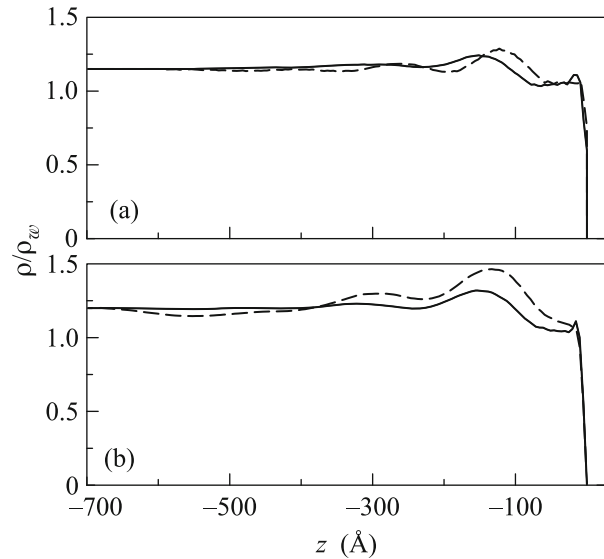


Fig. 5. Reconstructed distribution profiles $\rho(z)$ divided by the electron density in water $\rho_w = 0.333 \text{ electrons/\AA}^3$: (a) the surface of the sol of 7-nm particles (dashed line) immediately after the preparation of the sample and (solid line) after $\sim 170 \text{ h}$; (b) the surface of the sol of 12-nm particles (dashed line) immediately after the preparation of the sample and (solid line) after $\sim 120 \text{ h}$.

($d_0 \approx 20 \text{ \AA}$) peak of the electron density is also observed directly at the (air–silica sol) interface.

The behavior of the electron density distributions near the surface of the silica sol of 12-nm particles in Fig. 5b is similar. Immediately after the preparation of the sample (dashed line), the excess concentration of SiO_2 nanoparticles in the loose monolayer of nanoparticles is higher than the bulk value by a factor of ≈ 2 . In addition, a depleted layer is present at a depth of $\approx 550 \text{ \AA}$, where $\rho(z)$ is $\sim 6\%$ lower than the value in the bulk of this sol $\rho_b \approx 1.2\rho_w$. Thus, the concentration of particles in this layer is $\sim 40\%$ lower than the bulk value.

After $\sim 120 \text{ h}$ (the solid line), the deep enriched and depleted layers disappear and the concentration of nanoparticles in the loose monolayer decreases to ~ 1.4 of the bulk value. The total thickness of the separation region decreases from $\sim 700 \text{ \AA}$ to $\sim 400 \text{ \AA} \approx \Lambda_D$. A thin layer with the thickness $d_0 \sim 20 \text{ \AA}$ is also manifested on the surface.

Since all curves in Fig. 3 decrease as $\propto 1/q_z^6$, the further consideration implies the presence of the points of discontinuity of the first order in the structure. The reconstructed depth distributions of the electron density $\rho(z)$ divided by ρ_w are shown in Fig. 6.

In 1 h after preparation (Fig. 6a), the electron density at a depth up to 350 \AA ($\sim \Lambda_D$) is higher than the

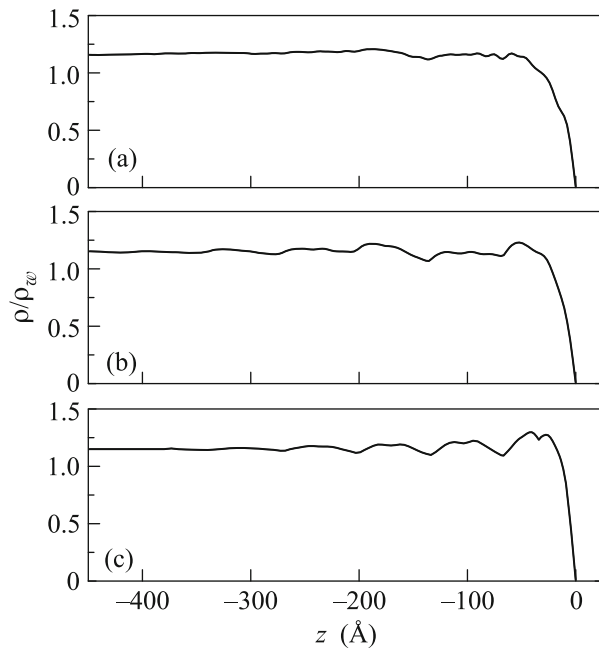


Fig. 6. Reconstructed distribution profiles $\rho(z)$ divided by the electron density in water $\rho_w = 0.333$ electrons/ \AA^3 for the DSPC lipid film on the surface of the sol of 7-nm particles (a) 1, (b) 24, and (c) 96 h after its deposition.

bulk value by 3–4% and the lipid film on the surface of the silica sol is apparently in a disordered state. The comparison of the structure of the surface layer of this sample with the above-considered surface of the sol indicates the disappearance of the feature associated with the loose monolayer of nanoparticles; i.e., the spreading of the lipid film is accompanied by a significant redistribution of particles.

After aging of the sample for 24 h, the reconstructed electron density distribution (Fig. 6b) at depth up to 350 \AA exhibits a quasiperiodic structure with a characteristic dimension of $d \approx 68$ \AA , which corresponds to the double length of the DSPC molecule (≈ 35 \AA).

Finally, after ~ 100 h, the profile $\rho(z)$ (Fig. 6c) demonstrates four pronounced lipid bilayers with the thickness $d = (68.1 \pm 0.9)$ \AA . The depth distribution of the electron density inside each bilayer is symmetric, which indicates a good ordering of molecules in it.

The angular dependences in Fig. 4 decrease as $\propto 1/q_z^4$; for this reason, the structure was reconstructed under the assumption of the zeroth order of points of discontinuity in the distribution of the polarizability. All reconstructed electron density distributions in Fig. 7 exhibit a structure of six to eight layers with a characteristic period of (66.7 ± 2.0) \AA , which corresponds to the thickness of the DSPC bilayer. The total thickness of the multilayer exceeds 500 \AA . A disor-

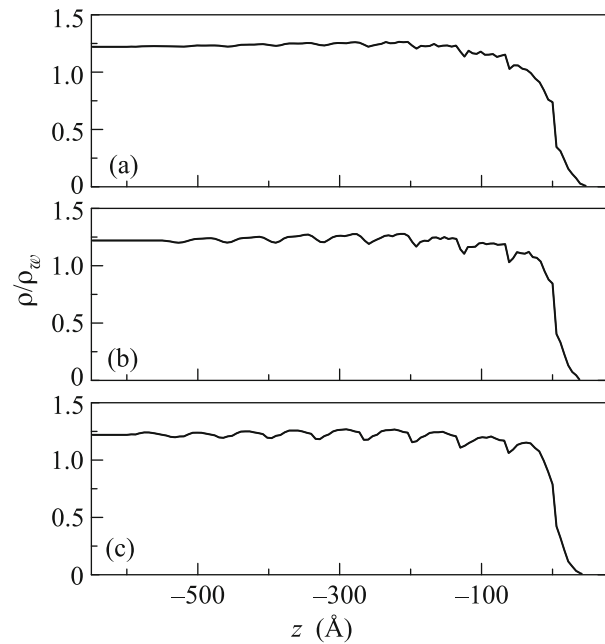


Fig. 7. Reconstructed distribution profiles $\rho(z)$ divided by the electron density in water $\rho_w = 0.333$ electrons/ \AA^3 for the DSPC film on the surface of the sol of 12-nm particles (a) 24, (b) 70, and (c) 200 h after its deposition.

dered layer with a low density and a thickness of about the DSPC monolayer ≈ 40 \AA is also present on the surface.

One day after the preparation of the sample (Fig. 7a), the electron density in bilayers near the air–phospholipid interface is significantly lower than that in bilayers near the silica sol substrate and its distribution inside individual bilayers is strongly asymmetric, which indicates their incomplete ordering. The area per lipid molecule for the most ordered bilayers at a depth of 250–400 \AA is estimated as $A = (37 \pm 2)$ \AA^2 .

After ~ 70 h (Fig. 7b), the integral electron density of bilayers hardly varies ($A = (36 \pm 2)$ \AA^2), but the interfaces between them become more pronounced. This indicates the lateral ordering of the structure of the lipid film.

Finally, after ~ 200 h (Fig. 7c), the electron density distribution within individual bilayers becomes symmetric at an unchanged integral electron density of the entire structure.

Thus, according to the reported data, a macroscopically flat structure is formed on the pure (air–silica sol) interface. The electron density profiles reconstructed with the model-independent approach are in agreement with the concept of the structure of the electric double layer on the surface of the hydrosol [17, 18]. The gradient of the surface potential on it appears owing to the difference between the potentials of

“electric image” forces for Na^+ cations and silica nanoparticles with a large negative charge ($\sim 10^3$ electrons) (macroions). Within several days of aging of the sample, nanoparticles in the surface layer of the silica sol are redistributed and a loose monolayer is formed. As a result, the distance between the plane of the closest approach of anion particles and the surface is $\sim 100 \text{ \AA}$, whereas Na^+ cations are accumulated immediately on the interface in a thin layer of the space charge with the thickness $d_0 \sim 20 \text{ \AA}$ [30, 31].

Our data also demonstrate the ordering with the time in the DSPC phospholipid multilayer deposited on the silica sol substrate. The characteristic thickness of the formed structure is $\sim \Lambda_D$, as in the case of the clean surface of the hydrosol.

During the first hour after the deposition of lipid, a thin layer with the thickness $\approx 130 \text{ \AA}$, which is separated from the substrate by a disordered material film with the thickness $\sim 200 \text{ \AA}$, is formed at the hydrosol–air interface. In this case, the feature on the reflectivity curve that is due to the loose monolayer of nanoparticles almost completely disappears. This indicates a significant rearrangement of the surface. Such a structure can be explained under the assumption that, e.g., the thin layer consists of three “liquid” lipid bilayers with the area per molecule $A = (55.7 \pm 0.7) \text{ \AA}^2$. This A value is in agreement with, e.g., an estimate for the area per molecule in the bilayer walls of vesicles [4].

During the next day, a quasiperiodic multilayer structure including five to eight partially ordered lipid bilayers is formed. Finally, several days ($(1-7) \times 10^5 \text{ s}$) after the preparation of the sample, the structure of the reconstructed profiles of the lipid multilayer does not change and a fine structure of monolayers can be identified inside individual bilayers. The average area per molecule in multilayers is $A = (36 \pm 2) \text{ \AA}^2$, which is noticeably smaller than its estimate $A_0 = (41.6 \pm 0.7) \text{ \AA}^2$ from diffraction data for crystalline bilayers [2, 6]. The comparison of A with A_0 gives the excess electron density averaged over the multilayer $\Gamma(A_0 - A)/A_0 = 60 \pm 20$ electrons per lipid molecule, which corresponds to four to eight Na^+ ions and H_2O molecules per DSPC molecule. The depth dependence of the distribution $\rho(z)$ for bilayers can be due both to filling defects and to inhomogeneous accumulation of Na^+ and H_2O in layers.

It is noteworthy that a monolayer is formed on the surface of the silica sol in the case of a low surface concentration of DSPC. In this case, the distance from the plane of closest approach between nanoparticles to the surface decreases to the thickness of the monolayer $\approx 35 \text{ \AA}$ and nanoparticles are condensed on its hydrophilic surface, at which the surface concentration of

particles is higher than the bulk value by a factor of ~ 2 [18]. In the considered case of a high surface concentration of DSPC molecules, the position of the plane of the closest approach of silica particles with respect to the surface is given by the thickness of the multilayer $\sim \Lambda_D$. In this case, any pronounced interface between it and the loose monolayer of nanoparticles is not observed, which indicates a decrease in their surface concentration.

A number of previous molecular dynamics calculations show that Na^+ ions can be introduced in phospholipid membranes, thus forming a positive surface potential [32–34]. However, such a mechanism can explain the excess electron density only in the bilayer directly adjacent to the substrate rather than in the entire multilayer.

An analogy can be seen between the formation of the surface structure with a transient process in an RC circuit, where the capacitance of the electric double layer C and the resistance of the multilayer R are connected in parallel to the source of the current of Na^+ ions, which is generated by electric image forces. The characteristic time of charging the capacitance is $\tau = RC \sim (1-7) \times 10^5 \text{ s}$, where $C \sim \epsilon_0 \epsilon_1 / \Lambda_D$ and $R \sim \rho \Lambda_D$ are the Helmholtz capacitance and the resistance of the multilayer per unit area, respectively. Consequently, the resistance of the DSPC bilayer per unit area is $\rho d \sim \tau d / (\epsilon_0 \epsilon_1) \approx (0.4-3) \times 10^8 \Omega \text{ m}^2$ at the static dielectric constant of the multilayer $\epsilon_1 \approx 2$. This ρd value is much lower than the resistance $10^{10} - 10^{13} \Omega \text{ m}^2$ previously obtained from the measurements of the ionic conductivity of unmodified phospholipid membranes [35]. In other words, the time τ for the observed structure is two to five orders of magnitude smaller than the expected value.

The electric field near the surface of the loose monolayer of nanoparticles, which orients the dipoles of DSPC molecules at the initial time, reaches $E > 10^9 \text{ V/m}$ [31]. The voltage drop ΔV across the thickness of the bilayer is $\Delta V = Ed > 7 \text{ V}$; i.e., the condition for its electric instability or electroporation is certainly satisfied ($\Delta V \geq 0.1 \text{ V}$) [36–39]. In this case, a certain porous structure is apparently formed in the multilayer through which the transport of Na^+ ions from the bulk of the hydrosol to the interface with air occurs more efficiently as compared to ohmic conductivity [40, 41]. In our opinion, such a mechanism of charge transport explains both a relatively small τ value and a high electron density in bilayers.

We are grateful to I.V. Kozhevnikov for stimulating discussions of the experimental results. This work was supported in part by the Russian Foundation for Basic Research (project no. 15-32-20935).

REFERENCES

1. E. Gorter and F. Grendel, *J. Exp. Med.* **41**, 439 (1925).
2. D. M. Small, *The Physical Chemistry of Lipids* (Plenum, New York, 1986).
3. *Phospholipids Handbook*, Ed. by G. Cevc (Marcel Dekker, New York, 1993).
4. N. Kučerka, M.-P. Mieh, and J. Katsaras, *Biochim. Biophys. Acta* **1808**, 2761 (2011).
5. O. S. Andersen and R. E. Koeppe II, *Ann. Rev. Biophys. Biomol. Struct.* **36**, 107 (2007).
6. A. M. Tikhonov, *JETP Lett.* **92**, 356 (2010).
7. A. M. Tikhonov, V. E. Asadchikov, and Yu. O. Volkov, *JETP Lett.* **102**, 478 (2015).
8. I. V. Kozhevnikov, *Nucl. Instrum. Methods Phys. Res. A* **508**, 519 (2003).
9. I. V. Kozhevnikov, L. Peverini, and E. Ziegler, *Phys. Rev. B* **85**, 125439 (2012).
10. A. V. Vinogradov and I. V. Kozhevnikov, *Tr. Fiz. Inst. im. P.N. Lebedeva, Ross. Akad. Nauk* **196**, 18 (1989).
11. I. V. Kozhevnikov, Doctoral (Phys. Math.) Dissertation (Shubnikov Inst. Crystallogr. RAS, Moscow, 2013).
12. Yu. O. Volkov, Cand. Sci. (Phys. Math.) Dissertation (Shubnikov Inst. Crystallogr. RAS, Moscow, 2015).
13. T. Graham, *Trans. R. Soc. London* **151**, 183 (1861).
14. J. W. Ryznar, in *Colloidal Chemistry: Theoretical and Applied*, Ed. by J. B. Alexander (Reinhold, New York, 1946), Vol. 6.
15. R. K. Iler, *The Chemistry of Silica* (Wiley-Interscience, New York, 1979).
16. J. Depasse and A. Watillon, *J. Colloid Interface Sci.* **33**, 430 (1970).
17. A. M. Tikhonov, *J. Chem. Phys.* **124**, 164704 (2006).
18. A. M. Tikhonov, *J. Phys. Chem. C* **111**, 930 (2007).
19. V. E. Asadchikov, V. V. Volkov, Yu. O. Volkov, K. A. Dembo, I. V. Kozhevnikov, B. S. Roshchin, D. A. Frolov, and A. M. Tikhonov, *JETP Lett.* **94**, 585 (2011).
20. V. V. Volkov, private commun.
21. V. E. Asadchikov, V. G. Babak, A. V. Buzmakov, Yu. P. Dorokhin, I. P. Glagolev, Yu. V. Zanevskii, V. N. Zryuev, Yu. S. Krivonosov, V. F. Mamich, L. A. Moseiko, N. I. Moseiko, B. V. Mchedlishvili, S. V. Savel'ev, R. A. Senin, L. P. Smykov, et al., *Instrum. Exp. Tech.* **48**, 364 (2005).
22. A. M. Tikhonov, *J. Phys. Chem. B* **110**, 2746 (2006).
23. H. Mohwald, *Ann. Rev. Phys. Chem.* **41**, 441 (1990).
24. J. Daillant, L. Bosio, B. Harzallah, and J. J. Benattar, *J. Phys. II* **1**, 149 (1991).
25. M. L. Schlossman, M. Li, D. M. Mitrovic, and A. M. Tikhonov, *High Perform. Polym.* **12**, 551 (2000).
26. A. M. Tikhonov and M. L. Schlossman, *J. Phys.: Condens. Matter* **19**, 375101 (2007).
27. M. Tolan, *Springer Tracts Mod. Phys.* **148**, 1 (1999).
28. J. Nocedal and S. Wright, *Numerical Optimization*, 2nd ed. (Springer, Berlin, 2006).
29. B. L. Henke, E. M. Gullikson, and J. C. Davis, *At. Data Nucl. Data Tables* **54**, 181 (1993).
30. A. M. Tikhonov, *J. Chem. Phys.* **126**, 171102 (2007).
31. A. M. Tikhonov, *J. Chem. Phys.* **130**, 024512 (2009).
32. S. A. Pandit, D. Bostick, and M. L. Berkowitz, *Biophys. J.* **82**, 1818 (2002).
33. M. Yi, H. Nymeyer, and H.-X. Zhou, *Phys. Rev. Lett.* **101**, 038103 (2008).
34. R. D. Porrasoa and J. J. L. Cascalesa, *Colloids Surf. B: Biointerfaces* **73**, 42 (2009).
35. A. Goldup, S. Ohki, and J. F. Danielli, *Recent Prog. Surf. Sci.* **3**, 193 (1970).
36. J. M. Crowley, *Biophys. J.* **13**, 711 (1973).
37. U. Zimmermann, G. Pilwat, and F. Riemann, *Biophys. J.* **14**, 881 (1974).
38. I. G. Abidor, V. B. Arakelyan, V. F. Pastushenko, M. R. Tarasevich, and L. V. Chernomordik, *Dokl. Akad. Nauk SSSR* **240**, 733 (1978).
39. R. Benz, F. Beckers, and U. Zimmerman, *J. Membr. Biol.* **48**, 181 (1979).
40. K. C. Melikov, V. A. Frolov, A. Shcherbakov, A. V. Samsonov, Yu. A. Chizmadzhev, and L. V. Chernomordik, *Biophys. J.* **80**, 1829 (2001).
41. M. Tarek, *Biophys. J.* **88**, 4045 (2005).

Translated by R. Tyapaev